Proceedings of the ASME 2022
International Design Engineering Technical Conferences and
Computers and Information in Engineering Conference
IDETC/CIE2021
August 14-17, 2022, St. Louis, Missouri

DETC2022-90021

CONTROL CO-DESIGN OPTIMIZATION OF NATURAL GAS POWER PLANTS WITH CARBON CAPTURE AND THERMAL STORAGE

Roberto Vercellino[1], Ethan Markey[1], Braden J. Limb[1], Maxwell Pisciotta[2], Joseph Huyett[1], Shane Garland[1], Todd Bandhauer[1], Jason C. Quinn[1], Peter Psarras[2], Daniel R. Herber[3]*

[1]Mechanical Engineering
Colorado State University
Fort Collins, CO 80523

[2]Chemical and Biomolecular Engineering
University of Pennsylvania
Philadelphia, PA 19104

[3]Systems Engineering
Colorado State University
Fort Collins, CO 80523

ABSTRACT

In this work, an optimization model was constructed to help address important design and operation questions for a novel system combining natural gas power plants with carbon capture and thermal storage. A control co-design (CCD) approach is taken where key plant sizing decisions (including storage capacities and energy transfer rates) and operational control (e.g., when to store and use thermal energy and operate the plant) are considered in an integrated manner using a simultaneous CCD strategy. The optimal design, as well as the operation of the system, are determined for an entire year (either all-at-once or through a moving prediction horizons strategy) in a large, sparse linear optimization problem. The results demonstrate both the need for optimal operation to enable a fair economic assessment of the proposed system as well as optimal sizing decisions due to sensitivity to a variety of scenarios, including different market conditions, site locations, and technology options.

Keywords: control co-design; optimal control; thermal energy storage; carbon capture; natural gas power plant

1 INTRODUCTION

International climate goals [1] and increasing penetration of renewable sources indicate a shift towards an energy market defined by fluctuating electricity demand and prices [2–6]. Within this prediction, an opportunity exists for alternative generation sources, which must operate flexibly to accommodate the market's variability and must also be close to carbon neutral to conform with the predicted penalties for the emission of CO_2 [3–7].

Natural gas combined cycle (NGCC) power plants, equipped with carbon capture (CC) technology, have been predicted to play a significant role in future grids [2, 7–9]. NGCC plants have proved to be flexible [2, 3, 5, 10, 10, 11], relatively inexpensive [5, 10], and are a consolidated technology already prevalent in the US and most advanced economies [2, 12]. On the other hand, while CC technology has demonstrated CO_2 capture rates larger than 90% [13], it still faces challenges preventing its commercial deployment, such as large capital investment and operation costs [12, 14], flexibility limitations [4, 15], and the parasitic load imposed by CC on the host system for solvent regeneration, which can decrease the net power output of the plant by as much as 10% [4, 7, 12, 16].

Solutions have been proposed to overcome these limitations and make CC profitable: some include coupling CC with external energy storage [7, 14], storing CO_2-rich solvent to limit CC's parasitic load at peak electricity prices [4, 6], and venting the CO_2 when more profitable than using CC [17]. A slightly different proposed solution consists in integrating NGCC and CC with hot thermal energy storage (HS) and cold thermal energy storage (CS) units. Energy can then be extracted from the NGCC or directly from the grid when the electricity prices are low and stored in both thermal energy storage (TES) units, and it can be discharged at peak prices from the HS to provide the heat required

*Corresponding author, daniel.herber@colostate.edu

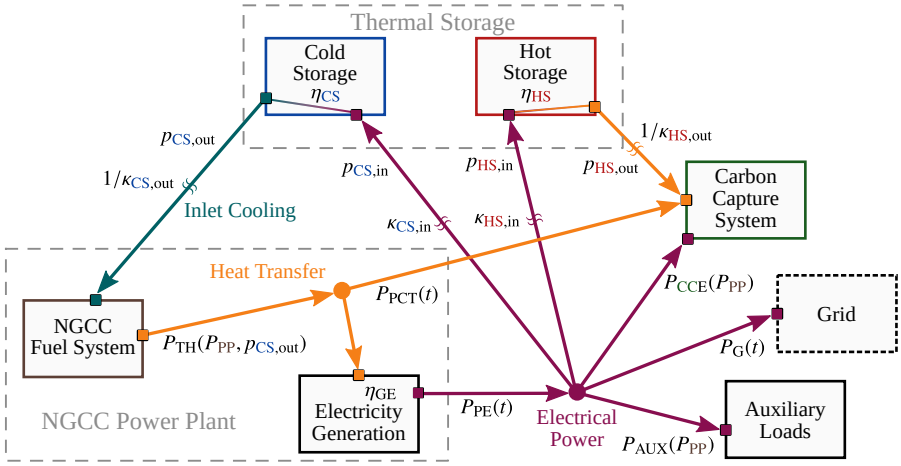

FIGURE 1: Key subsystems and the flows between them.

for CC and from the CS to chill the inlet air to the NGCC an increase the plant's net power output. The implementation of TES technology would retain the output flexibility of NGCC power plants while allowing CC to operate at steady-state; it would deconstraint the NGCC plant beyond nominal operation output during peak price periods by utilizing stored energy from the TES for solvent regeneration and air pre-chilling [18, 19].

Although a promising concept, the complexities of an NGCC power plant coupled with CC, HS, and CS pose great design and control challenges: for profitable implementation, each of the aforementioned subsystems (NGCC, CC, HS, CS) needs to simultaneously operate in response to time-varying external signals such as electricity and fuel price, CO_2 tax, and ambient temperature. In addition, sizing decisions accompanying the realization of such systems are strictly dependent on their day-to-day operation. Accordingly, a control co-design (CCD) optimization approach can effectively be leveraged to simultaneously optimize the physical design and control strategy of this system [20]. Existing literature involving optimal design and control of similar projects has focused on photovoltaic and wind energy systems integrated with battery storage [21–23], power generation systems coupled with energy storage [24–28], or alternatively it has looked at the optimization of NGCC power plants coupled with CC [6, 17, 29, 30], but never with TES.

Here we present a CCD optimization model tailored to maximize the net present value (NPV) of a NGCC power plant coupled with CC, HS, and CS units in different scenarios. The model has been used to assess 17 different TES configurations with various CC technologies in hundreds of electricity market scenarios, as well as different geographical locations defined by their unique temperature profiles [18, 19]. While using NPV to evaluate the system over its lifetime, the model leverages an efficient formulation and optimization techniques to represent the plant's operation with high resolution. The optimization problem can be posed as a simultaneous CCD linear program when assuming perfect foresight of the provided techno-economics signals. However, when limited information on the signals is imposed to resemble more realistic market conditions, a nested approach is chosen, and the overall problem is solved as a sequence of linear subproblems.

The rest of the paper is organized as follows: Sec. 2 describes the CCD problem formulation; Sec. 3 discusses the specific optimization methods utilized; and Sec. 4 presents the results of several different case studies demonstrating the capabilities of the CCD approach to make sound economic judgments of the proposed system. Finally, Sec. 5 presents the conclusions.

2 PROBLEM FORMULATION

In this section, the dynamic optimization model of an NGCC power plant (PP), coupled with CC, HS, and CS units as well as the NPV calculation are presented. Because of the dynamic nature of the model, many of the problem variables depend on time t. In addition, some of the model variables also depend on ambient temperature T_0, which is provided to the model as a time-dependent signal $T_0(t)$. Figure 1 is a high-level representation of each of the subsystems and the energy flows between them. Different arrow colors in the image represent different forms or power, including heat transfer, electrical power, and inlet-cooling power from discharging the CS (which increases the efficiency and capacity of the PP). Many of the specific parameters used in the case study are in App. A.

2.1 Thermal Energy Storage

Plant Variables and Constraints—There are three plant variables associated with each of the TES units:

$$\boldsymbol{p} = \left[\Sigma_{HS}\ P_{HS,in}\ P_{HS,out}\ \Sigma_{CS}\ P_{CS,in}\ P_{CS,out}\right]^T \tag{1}$$

where (Σ_{HS}, $P_{HS,in}$, $P_{HS,out}$) are the HS storage capacity, maximum energy transfer rate into the HS, and maximum energy transfer rate out of the HS, respectively, and (Σ_{CS}, $P_{CS,in}$, $P_{CS,out}$) are the equivalent plant variables for the CS.

To ensure that the hot and cold TES capacities are non-negative, we impose the following constraints:

$$\Sigma_{HS} \geq 0 \qquad \Sigma_{CS} \geq 0 \tag{2}$$

where no thermal storage is an option if the lower bound is active.

Since the HS configuration's purpose to take over the CC reboiler duty, we assume that the maximum energy rate from the HS is the provided nominal design; to avoid technical limitations, we make a similar assumption for the CS. In addition, we enforce the energy rate from the TES units to be non-negative. These points are summarized with the following constraints:

$$0 \leq P_{HS,out} \leq \bar{P}_{HS,out} \qquad 0 \leq P_{CS,out} \leq \bar{P}_{CS,out} \tag{3}$$

Similarly, there are technical limitations imposed onto the maximum charging rates, as well as non-negativity:

$$0 \leq P_{HS,in} \leq \bar{P}_{HS,in} \qquad 0 \leq P_{CS,in} \leq \bar{P}_{CS,in} \tag{4}$$

Control Variables and Constraints—As TES units, both the HS and CS can dynamically store and release thermal power; these are the four control variables:

$$\boldsymbol{u}_T(t) = \left[p_{HS,in}(t)\ p_{CS,in}(t)\ p_{HS,out}(t)\ p_{CS,out}(t)\right]^T \tag{5}$$

where ($p_{HS,in}$, $p_{CS,in}$) are the input power to the HS and the CS from the electricity generator, respectively; $p_{HS,out}$ is the output power from the HS to the CC; and $p_{CS,out}$ is the output power from the CS to the PP module.

To ensure that the non-negative power inputs are less than the limits, we include the following inequality constraints:

$$0 \leq p_{HS,in}(t) \leq \mu_{HS,in}(T_0) \cdot P_{HS,in} \tag{6a}$$
$$0 \leq p_{CS,in}(t) \leq \mu_{CS,in}(T_0) \cdot P_{CS,in} \tag{6b}$$

where ($\mu_{HS,in}$, $\mu_{CS,in}$) define the fraction of the nominal power input available at the current temperature T_0. Similar constraints are imposed on the allowed power outputted from the TES units:

$$0 \leq p_{HS,out}(t) \leq \mu_{HS,out}(T_0) \cdot P_{HS,out} \tag{7a}$$
$$0 \leq p_{CS,out}(t) \leq \mu_{CS,out}(T_0) \cdot P_{CS,out} \tag{7b}$$

where ($\mu_{HS,out}$, $\mu_{CS,out}$) similarly constraint the effective discharging power available to the TES units at any time.

States and Constraints—There is one key state for each of the two TES units, namely the current amount of stored thermal energy. The differential equations are simple balances between the input and output powers for each:

$$\dot{E}_{HS} = \kappa_{HS,in} \cdot p_{HS,in}(t) - \kappa_{HS,out} \cdot p_{HS,out}(t) \tag{8a}$$
$$\dot{E}_{CS} = \kappa_{CS,in} \cdot p_{CS,in}(t) - \kappa_{CS,out} \cdot p_{CS,out}(t) \tag{8b}$$

where ($\kappa_{HS,in}$, $\kappa_{CS,in}$) are the coefficients converting the electricity subtracted from the PP to thermal power to the TES units; whereas ($\kappa_{HS,out}$, $\kappa_{CS,out}$) indicate the conversion from the TES discharging electrical power to the thermal power flowing out of the TES units. The initial states of the thermal storage subsystems are:

$$E_{HS}(t_0) = E_{HS,0} \qquad E_{CS}(t_0) = E_{CS,0} \tag{9}$$

To ensure that the thermal energy storage is positive and below the maximum level allowed, we finally include:

$$0 \leq E_{HS}(t) \leq \Sigma_{HS} \qquad 0 \leq E_{CS}(t) \leq \Sigma_{CS} \tag{10}$$

2.2 Natural Gas Combined Cycle Power Plant

Control Variables and Constraints—There is one control optimization variable associated with the NGCC power plant, which represents the requested power output:

$$\boldsymbol{u}_P(t) = \left[p_{PP}(t)\right]^T \tag{11}$$

We include a constraint to ensure the requested power output to be non-negative and less than the allowed limits:

$$0 \leq p_{PP}(t) \leq \mu_{PP}(T_0) \cdot \bar{P}_{PP} \tag{12}$$

where $\bar{P}_{PP}$ is the provided maximum nominal power of the NGCC and μ_{PP} defines the fraction of power available depending on the ambient temperature.

States and Constraints—The requested power output in Eq. (11) is used in a dynamic equation describing the power level of the PP, a state variable in the problem:

$$\dot{P}_{PP}(t) = \frac{1}{\tau_{PP}}\Big(-P_{PP}(t) + p_{PP}(t)\Big) \tag{13}$$

where (τ_{PP}) is the ramp rate of the PP. The initial state of the PP is:

$$P_{PP}(t_0) = P_{PP,0} \tag{14}$$

We also include a constraint to ensure the effective power output to be non-negative and less than the allowed limits:

$$0 \leq P_{PP}(t) \leq \mu_{PP}(T_0) \cdot \bar{P}_{PP} \tag{15}$$

During combined operation of the PP and TES, we would like to limit charging and discharging of TES to only when the PP

is operating, so we include the following inequality constraints:

$$p_{\mathrm{HS,in}}(t) \le P_{\mathrm{PP}}(t) \qquad p_{\mathrm{CS,in}}(t) \le P_{\mathrm{PP}}(t) \tag{16a}$$

$$p_{\mathrm{HS,out}}(t) \le P_{\mathrm{PP}}(t) \qquad p_{\mathrm{CS,out}}(t) \le P_{\mathrm{PP}}(t) \tag{16b}$$

so energy can only flow to or from any TES element if $P_{\mathrm{PP}} > 0$.

Intermediate Functions—From a combination of plant and control variables, states, and problem parameters from the HS, CS, and PP, the instantaneous fuel consumption of the PP is:

$$m_f(t) = \rho_f \cdot \mu_f(T_0) \cdot P_{\mathrm{PP}}(t) + \Delta\rho_f \cdot \mu_{\Delta f}(T_0) \cdot p_{\mathrm{CS,out}}(t) \tag{17}$$

where ρ_f is the nominal conversion factor between power output generated by the NGCC and fuel consumed, and $\Delta\rho_f$ is the same quantity but associated with discharging the CS. (μ_f, $\mu_{\Delta f}$) are factors affecting these quantities depending on the ambient temperature. Equation (17) represents a fundamental intermediate function in the calculation of the expenses associated with running the system in Eq. (28b).

2.3 Carbon Capture

The CC subsystem is implemented such that it is always operating when the PP is operating. Therefore, all its characteristics are dependent on the signals described in the previous subsection.

One of the key aspects of the CC subsystem is the instantaneous CO_2 capture rate, which is:

$$\beta_{\mathrm{C}}(t) = c_{\mathrm{n}} \cdot \mu_c(T_0) \cdot P_{\mathrm{PP}}(t) - \Delta c_{\mathrm{d}} \cdot \mu_{\Delta c}(T_0) \cdot p_{\mathrm{CS,out}}(t) \tag{18}$$

where c_{n} is the percentage of carbon captured from the flue gas when the PP runs in the neutral state, and Δc_{d} is the decrease in capture when the CS is being discharged. (μ_c, $\mu_{\Delta c}$) describe how these nominal capture rates are affected by ambient temperature. Here, we are assuming that total amount of CO_2 generated by the whole system is directly proportional to the fuel burned, m_f from Eq. (17), according to the conversion coefficient α_{C}. It follows that of the total CO_2 generated, the portion captured and emitted into the atmosphere are respectively:

$$m_{\mathrm{C,in}}(t) = m_f(t) \cdot \alpha_{\mathrm{C}} \cdot \beta_C(t) \tag{19a}$$

$$m_{\mathrm{C,out}}(t) = m_f(t) \cdot \alpha_{\mathrm{C}} \cdot \left(1 - \beta_C(t)\right) \tag{19b}$$

As currently described, ($m_{\mathrm{C,in}}$, $m_{\mathrm{C,out}}$) are nonlinear terms in the objective function. We have found that we can maintain the linearity without virtually losing any accuracy in the solution by approximating the expressions above using two known points of operation: 1) the neutral phase of the PP, and 2) the discharging phase of the CS. So we rewrite Eq. (19) as:

$$\hat{m}_{\mathrm{C,in}}(t) = \underline{\rho}_{\mathrm{C,in}}(T_0) \cdot P_{\mathrm{PP}}(t) + \Delta\rho_{\mathrm{C,in}}(T_0) \cdot p_{\mathrm{CS,out}}(t) \tag{20a}$$

$$\hat{m}_{\mathrm{C,out}}(t) = \underline{\rho}_{\mathrm{C,out}}(T_0) \cdot P_{\mathrm{PP}}(t) + \Delta\rho_{\mathrm{C,out}}(T_0) \cdot p_{\mathrm{CS,out}}(t) \tag{20b}$$

where ($\underline{\rho}_{\mathrm{C,in}}$, $\underline{\rho}_{\mathrm{C,out}}$) are the CO_2 captured and emitted by the whole system in neutral mode per unit power generated:

$$\underline{\rho}_{\mathrm{C,in}} = \alpha_{\mathrm{C}} \cdot \rho_f \cdot \mu_f(T_0) \cdot c_{\mathrm{n}} \cdot \mu_c(T_0) \tag{21a}$$

$$\underline{\rho}_{\mathrm{C,out}} = \alpha_{\mathrm{C}} \cdot \rho_f \cdot \mu_f(T_0) \cdot (1 - c_{\mathrm{n}} \cdot \mu_c(T_0)) \tag{21b}$$

and ($\Delta\rho_{\mathrm{CO_2,in}}$, $\Delta\rho_{\mathrm{CO_2,out}}$) are the coefficients describing the linear trajectory from the neutral phase to the maximum discharging of the CS, per unit power generated from discharging the CS. There are thermal and electrical power requirements, respectively P_{CCT} and P_{CCE}, to run the CC unit, which depend on the technology implemented, the PP power level, and the nominal capture percentage $\bar{\beta}_{\mathrm{C}}$:

$$P_{\mathrm{CCT}} = P_{\mathrm{CCT}}(P_{\mathrm{PP}}, \bar{\beta}_{\mathrm{C}}) \qquad P_{\mathrm{CCE}} = P_{\mathrm{CCE}}(P_{\mathrm{PP}}, \bar{\beta}_{\mathrm{C}}) \tag{22}$$

where P_{CCE} is electrical power directly extracted from the PP output, while P_{CCT} is thermal power in the form of steam, which is either also extracted from the PP or is provided by discharging the HS. It follows that the power that must be extracted from the PP is whatever fraction of P_{CCT} that is not provided by the HS:

$$P_{\mathrm{PCT}}(t) = P_{\mathrm{CCT}}(P_{\mathrm{PP}}, \bar{\beta}_{\mathrm{C}}) - \eta_{\mathrm{HS}} \cdot p_{\mathrm{HS,out}}(t) \tag{23}$$

where η_{HS} accounts for any efficiency losses.

2.4 Electricity Generation

The electricity generated by the system is the primary source of revenue driving the NPV objective. The corrected thermal power outputted from the PP, here indicated as P_{TH}, depends on the PP level and on the discharging of the CS:

$$P_{\mathrm{TH}}(t) = P_{\mathrm{PP}}(t) + \eta_{\mathrm{CS}} \cdot p_{\mathrm{CS,out}}(t) \tag{24}$$

where η_{CS} represents any efficiency losses from discharging the CS. The gross electricity generated is then:

$$P_{\mathrm{PE}}(t) = \eta_{\mathrm{GE}} \cdot \left(P_{\mathrm{TH}}(t) - P_{\mathrm{PCT}}(t)\right) \tag{25}$$

where η_{GE} is the efficiency of conversion between thermal and electrical power, and P_{PCT} is the thermal power diverted to the CC as in Eq. (23). From the gross electrical power generated by the system, a fraction is diverted to the CC in Eq. (22); a fraction might be sent to charge the TES units; finally, some power is required to satisfy the system's auxiliary loads P_{AUX}, which can depend on the state of the PP. Therefore, the net power outputted to the grid is:

$$P_{\mathrm{G}} = P_{\mathrm{PE}} - P_{\mathrm{CCE}} - p_{\mathrm{HS,in}} - p_{\mathrm{CS,in}} - P_{\mathrm{AUX}} \tag{26}$$

2.5 Techno-Economic Analysis

Revenue and Expenses—v_{rev} is the revenue gained by outputting power to the grid P_{G} calculated in Eq. (26) at the current

electricity price c_{elec}:

$$v_{\text{rev}}(t) = c_{\text{elec}}(t) \cdot P_{\text{G}}(t) \tag{27}$$

and v_{exp} represents the expenses of the system, which are divided in cost of fuel v_{fuel} and other operation costs v_{op}:

$$v_{\text{exp}}(t) = v_{\text{fuel}}(t) + v_{\text{op}}(t) \tag{28a}$$
$$v_{\text{fuel}}(t) = c_{\text{fuel}}(t) \cdot m_f(t) \tag{28b}$$
$$v_{\text{op}}(t) = c_{\text{CO}_2} \cdot \hat{m}_{\text{C,out}}(t) + C_{\text{VOM}}(t) + C_{\text{FOM}}(t) \tag{28c}$$

where $(m_f, \hat{m}_{\text{C,out}})$ are the instantaneous fuel consumed and CO_2 emitted into the atmosphere by the system, respectively, as described in Eqs. (17) and (20b). Conversely, c_{fuel} is the instantaneous fuel cost, while c_{CO_2} is the selected carbon tax. C_{VOM} encompasses all the additional costs which depend on running each of the subsystems:

$$\begin{aligned} C_{\text{VOM}}(t) = {} & c_{\text{PP,VOM}} \cdot P_{\text{PP}}(t) + c_{\text{CC,VOM}} \cdot \hat{m}_{\text{CO}_2\text{,in}}(t) \cdots \\ & + c_{\text{HS,VOM}} \cdot \left(p_{\text{HS,in}}(t) + p_{\text{HS,out}}(t)\right) \cdots \\ & + c_{\text{CS,VOM}} \cdot \left(p_{\text{CS,in}}(t) + p_{\text{CS,out}}(t)\right) \end{aligned} \tag{29}$$

where the first term depends on the PP power level P_{PP}; the second term depends on the CO_2 captured by the system from Eq. (20a); the last two terms are associated with the power charging and discharged by both TES units. Finally, C_{FOM} includes the operation costs from each of the subsystems, independent of their utilization:

$$\begin{aligned} C_{\text{FOM}}(t) = {} & c_{\text{PP,FOM}} + c_{\text{CC,FOM}} \cdots \\ & + c_{\text{HS,FOM}} \cdot \left(P_{\text{HS,in}} + P_{\text{HS,out}}\right) \cdots \\ & + c_{\text{CS,FOM}} \cdot \left(P_{\text{CS,in}} + P_{\text{CS,out}}\right) \cdots \\ & + c_{\text{HS,TES,FOM}} \cdot \Sigma_{\text{HS}} + c_{\text{CS,TES,FOM}} \cdot \Sigma_{\text{CS}} \end{aligned} \tag{30}$$

Capital Costs—The system's capital costs C_{cap} are:

$$C_{\text{cap}}(\boldsymbol{p}) = C_{\text{PP}} + C_{\text{CC}} + C_{\text{HS}}(\boldsymbol{p}) + C_{\text{CS}}(\boldsymbol{p}) \tag{31}$$

where $(C_{\text{PP}}, C_{\text{CC}})$ are the fixed capital investment to realize the PP and the CC subsystems, while $(C_{\text{HS}}, C_{\text{CS}})$ are the costs for the TES units and depend on $\boldsymbol{p}$:

$$C_{\text{HS}}(\boldsymbol{p}) = c_{\text{HS,in}} \cdot P_{\text{HS,in}} + c_{\text{HS,out}} \cdot P_{\text{HS,out}} + c_{\text{HS,TES}} \cdot \Sigma_{\text{HS}} \tag{32a}$$
$$C_{\text{CS}}(\boldsymbol{p}) = c_{\text{CS,in}} \cdot P_{\text{CS,in}} + c_{\text{CS,out}} \cdot P_{\text{CS,out}} + c_{\text{CS,TES}} \cdot \Sigma_{\text{CS}} \tag{32b}$$

where $(c_{\text{HS,in}}, c_{\text{HS,out}})$ represent the capital costs scaling with the desired charging and discharging power capacity of the HS unit, while $c_{\text{HS,TES}}$ is the cost of the HS medium. Conversely, $(c_{\text{CS,in}}, c_{\text{CS,out}}, c_{\text{CS,TES}})$ represent the similar costs for the CS. The following subsection analyzes more in depth the economic model for calculating the net present value of the overall system, the primary metric of interest.

Net Present Value Calculation—NPV was selected as main economic indicator for the proposed system, because it represents the return on investment over its entire lifetime [31]. Other indicators, such as levelized-cost of electricity (LCOE), are typically used for power generation systems, but due to the arbitrage nature of the system being evaluated, they would not accurately represent its benefit.

In simplified terms, NPV is the difference between the present value of cash inflows and the present value of cash outflows during a period of time (typically the loan term L_t). To convert future values into a present value, a discount factor DF is used, which depends on the year evaluated y and the selected rate of return IRR:

$$DF(y) = \frac{1}{(1 + IRR)^y} \tag{33}$$

Assuming the capital investment to build the plant is made before the start of the operation, an equation to calculate NPV is:

$$NPV = V_{\text{income}} - C_{\text{cap}} \tag{34}$$

The income generated from the system V_{income} is the summation of the profit made discounted over the system's lifetime:

$$V_{\text{income}} = \sum_{y=1}^{L_t} \Big(V_{\text{rev}}(y) - V_{\text{exp}}(y)\Big) \cdot DF(y) \tag{35}$$

where $(V_{\text{rev}}, V_{\text{exp}})$ are respectively the revenue and expenses from running the system, which are based on Eq. (27) and (28a) and are obtained upon integration over a year of operation:

$$V_{\text{rev}}(y) = \int_0^{T_{\text{year}}} \left[v_{\text{rev}}(t) \cdot (1 + i_e)^{y-1}\right] \mathrm{d}t \tag{36a}$$
$$V_{\text{exp}}(y) = \int_0^{T_{\text{year}}} \left[v_{\text{fuel}}(t) \cdot (1 + i_f)^{y-1} + v_{\text{op}}(t)\right] \mathrm{d}t \tag{36b}$$

To reduce the size of the problem, in this analysis we assume the control strategy of the plant over its lifetime is identical to that of the first year of operation (from $t = 0$ to T_{year}). However, we reflect the expected annual increase in electricity and fuel prices with the factors (i_e, i_d). We use Eq. (36) to rewrite Eq. (35) as:

$$V_{\text{income}} = \int_0^{T_{\text{year}}} \sum_{y=1}^{L_t} \begin{bmatrix} v_{\text{rev}}(t) \\ -v_{\text{fuel}}(t) \\ -v_{\text{op}}(t) \end{bmatrix}^T \begin{bmatrix} r_e^{y-1} \\ r_f^{y-1} \\ r_d^{y-1} \end{bmatrix} \mathrm{d}t \tag{37}$$

$$\text{where: } r_e = \frac{1 + i_e}{1 + IRR} \quad r_d = \frac{1 + i_f}{1 + IRR} \quad r_d = \frac{1}{1 + IRR}$$

The non-constant terms within the sum in Eq. (37) resemble a

geometric series for which a closed-form solution exists [32]:

$$\sum_{i=1}^{n} aq^{i-1} = \frac{a(1-q^n)}{1-q} \tag{38}$$

which allows us to rewrite the NPV of the system in closed form:

$$NPV = -C_{\text{cap}} + \int_0^{T_{\text{year}}} \begin{bmatrix} v_{\text{rev}}(t) \\ -v_{\text{fuel}}(t) \\ -v_{\text{op}}(t) \end{bmatrix}^T \begin{bmatrix} R_e \\ R_f \\ R_d \end{bmatrix} \mathrm{d}t \tag{39}$$

$$\text{where: } R_e = \frac{1-r_e^{L_t}}{1-r_e} \quad R_f = \frac{1-r_f^{L_t}}{1-r_f} \quad R_d = \frac{1-r_d^{L_t}}{1-r_d}$$

2.6 Objective Function and Summary

We now provide a brief summary of the CCD problem described in the previous sections. We start by reporting the six total plant design optimization variables first presented in Eq. (1):

$$\boldsymbol{p} = \left[\Sigma_{\text{HS}} \; P_{\text{HS,in}} \; P_{\text{HS,out}} \; \Sigma_{\text{CS}} \; P_{\text{CS,in}} \; P_{\text{CS,out}}\right]^T \tag{40}$$

Additionally, there are four control variables associated with operating the TES units defined in Eq. (5), and one control variable for the NGCC from Eq. (11). Therefore, there is a total of five open-loop controls optimized in the problem:

$$\boldsymbol{u}(t) = \left[p_{\text{HS,in}}(t) \; p_{\text{CS,in}}(t) \; p_{\text{HS,out}}(t) \; p_{\text{CS,out}}(t) \; p_{\text{PP}}(t)\right]^T \tag{41}$$

Finally, there are three state variables:

$$\boldsymbol{\xi}(t) = \left[E_{\text{HS}}(t) \; E_{\text{CS}}(t) \; P_{\text{PP}}(t)\right]^T \tag{42}$$

which respectively describe the HS, CS, and PP levels, and whose linear time-invariant (LTI) dynamic equations are shown in Eqs. (8) and (13). Additionally, there a several inequality and equality constraints (both path and boundary types), but all are linear. Finally, the linear objective function of the problem is to maximize NPV of the system in Eq. (39). The unconstrained objective function is:

$$\underset{\boldsymbol{u},\boldsymbol{\xi},\boldsymbol{p}}{\text{maximize}} \;\; NPV(t, T_0, \boldsymbol{u}, \boldsymbol{\xi}, \boldsymbol{p}) \tag{43}$$

Overall, the problem is a linear dynamic optimization problem; all constraints are linear and, due to the approximation described in Sec. 2.3, the objective is linear as well. Such problems can be efficiently solved using linear solvers [33]. So, much of the complexity in solving this particular CCD problem comes from the complexity of a variety of intermediate functions, combined with a multitude of time-varying environmental inputs and large timescales (and resulting large optimization problem) to consider.

3 OPTIMIZATION STRATEGY CONSIDERATIONS

Here we discuss additional aspects surrounding the practical construction and solving of the linear CCD optimization problem from the previous section.

3.1 Approximations

One approximation was already discussed in Sec. 2.3 where a quadratic expression was linearized to maintain a linear objective function. The maximum error in calculating the NPV found by comparing the exact and linearization results over many real scenarios was never found to be larger than 0.01%. While a quadratic objective function would still result in a LQDO problem, it was determined that the relatively small error and efficiency of the approximation was worth its implementation.

3.2 Problem Discretization

To solve the dynamic optimization posed in Sec. 2, direct transcription (DT) is used [33–35]. In this case, the resulting finite-dimensional optimization is a large, sparse linear program and was constructed using the open-source MATLAB software DTQP [36]. Then, MATLAB's linprog solver using the interior-point method [37] was found to be quite effective at solving the resulting linear program.

The time mesh was selected to be at hourly intervals as it is a reasonable assumption for the frequency at which control decisions (e.g., power plant's power level would be changed) are made during realistic operation. The control decisions over these hourly intervals were assumed to be constant. With constant controls and linear dynamics, the zero-order hold (ZOH) method was used to discretize the dynamic constraints since there would be no discretization error [33]; a basic composite Euler forward method was chosen for quadrature. The ZOH method is particularly efficient to implement if matrices are time invariant. However, There are several locations in the formulation where time (really temperature) dependence would be useful, such as Eqs. (8) and (13).

This was particularly true for the state equations governing the flow of energy to and from the TES units described in Eq. (8) since it is desirable to allow the control variables ($p_{\text{HS,in}}$, $p_{\text{CS,in}}$, $p_{\text{HS,out}}$, $p_{\text{CS,out}}$) to be temperature-dependent to limit the amount of power flowing in or out of the TES units at certain temperatures – see Sec. 4.2 for more details. While an intuitive way is directly expressing these values as time-varying, this would result in a time-varying linear (LTV) system, slowing down the problem construction step. An alternative but equivalent formulation was utilized by instead imposing time-dependent upper bounds on the relevant controls. This is demonstrated in the following notional example:

$$\dot{\xi} = a(t) \cdot u(t) \text{ and } 0 \le u(t) \le 1 \qquad \text{(LTV case)} \tag{44a}$$

$$\dot{\xi} = \bar{u}(t) \text{ and } 0 \le \bar{u}(t) \le a(t) \qquad \text{(LTI case)} \tag{44b}$$

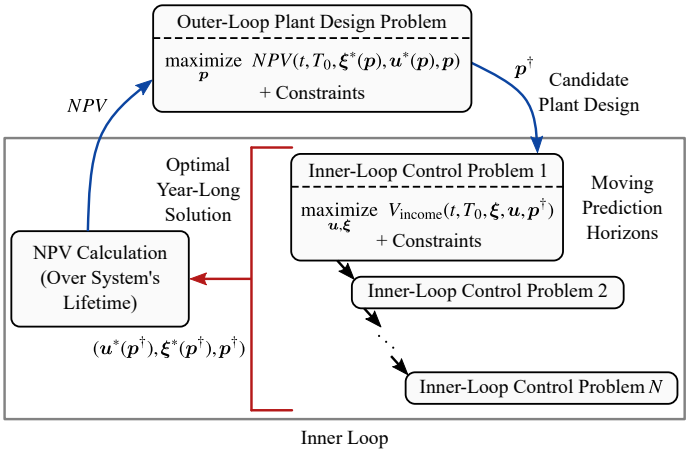

FIGURE 2: Overview of the nested control co-design optimization architecture for the moving prediction horizons approach.

In this formulation, Eqs. (6) and (7) are the relevant control constraints while Eq. (8) are expressed without any direct dependence on T_0. When the upper bounds in Eqs. (6) and (7) are active, it can easily be shown that Eq. (8) assume the desired temperature-dependence.

3.3 Moving Prediction Horizons

As currently posed, the open-loop optimal control problem can be solved for any desired time horizon. As discussed in Sec. 2.5, the goal is to obtain results for one year of operation for use in the NPV calculations. This can be accomplished with a single optimization problem using an entire year's worth of data.

However, despite this capability, solving a single horizon problem is not a realistic scenario as key environmental signals are not known with certainty so far into the future. In the real markets, signals such as electricity and fuel prices and ambient temperature are known to utility operators with reasonable accuracy only with limited foresight (e.g., 24 hours of future information [38]). To reflect this imperfect knowledge, which is crucial when determining the most profitable control strategy, the problem is also posed in as a sequence of shorter moving "prediction horizons" where information is known. Based on notions of model predictive control (MPC), this approach entails leveraging the knowledge of the future signals, despite being limited, to construct a tentative control strategy that is then updated when new information about the signals is available [39]. There are examples in the literature where similar control strategies based on limited future knowledge are applied to residential heating and cooling systems coupled with storage [27, 28].

When the moving horizons approach is taken, a nested CCD strategy formulation is used because separation is needed between the plant and control decisions [20, 40, 41]. As shown in Fig. 2, the inner loop is formulated as a sequence of control sub-

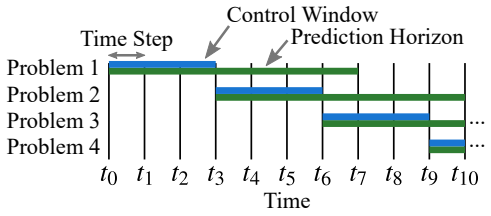

FIGURE 3: Moving prediction horizons and control window illustration.

problems whose objective is to maximize the income generated by the system in Eq. (35) with respect to the states and controls $(\boldsymbol{\xi}, \boldsymbol{u})$ for fixed plant variables $\boldsymbol{p}^\dagger$. The inner-loop solutions are then used in the objective function of the outer loop, which attempts to maximize NPV in Eq. (39).

Trade-offs in both control window and prediction horizon lengths (see Fig. 3) are explored in Sec. 4.3. The prediction horizon is the amount of time in the future information is known and includes many operational decisions to be made (e.g., from points t_0 to t_7 in the figure). The control window is the initial part of the prediction horizon that is implemented. After solution in the control window is implemented, the next optimization problem is solved starting where the previous control window ended. Understanding these trade-offs will help lead to implementable CCD-informed control solutions [42].

4 RESULTS AND DISCUSSION

The following section presents several sets of results generated using the optimization model introduced in the previous sections with the purpose of validating its implementation and demonstrating some of its capabilities. Several TES technology configurations operating in different market scenarios and geographical locations will be examined. A detailed thermodynamic analysis has been conducted to generate the technical parameters identifying each of the TES configurations listed in App. A.1, which have then been modeled as integrated with the NGCC plant coupled with a Cansolv CC system [13] presented in the National Energy Technology Laboratory's (NETL) 2019 report (B31B) [43]. Further details into the derivations of these parameters are in other publications [18, 19].

The electricity and fuel prices and corresponding CO_2 tax used for this work represent future grid scenarios and have been generated by capacity expansion models built by Princeton University and NREL [44, 45]. Temperature data from six of the more representative cities in the US was pulled from NREL's National Solar Radiation Database from 2018 [46]. Finally, the economic and financial values assumed for the calculation of NPV in these studies are reported in App. A.2.

When solving the problem using the simultaneous strategy for an entire year, the setup and solving of the required linear

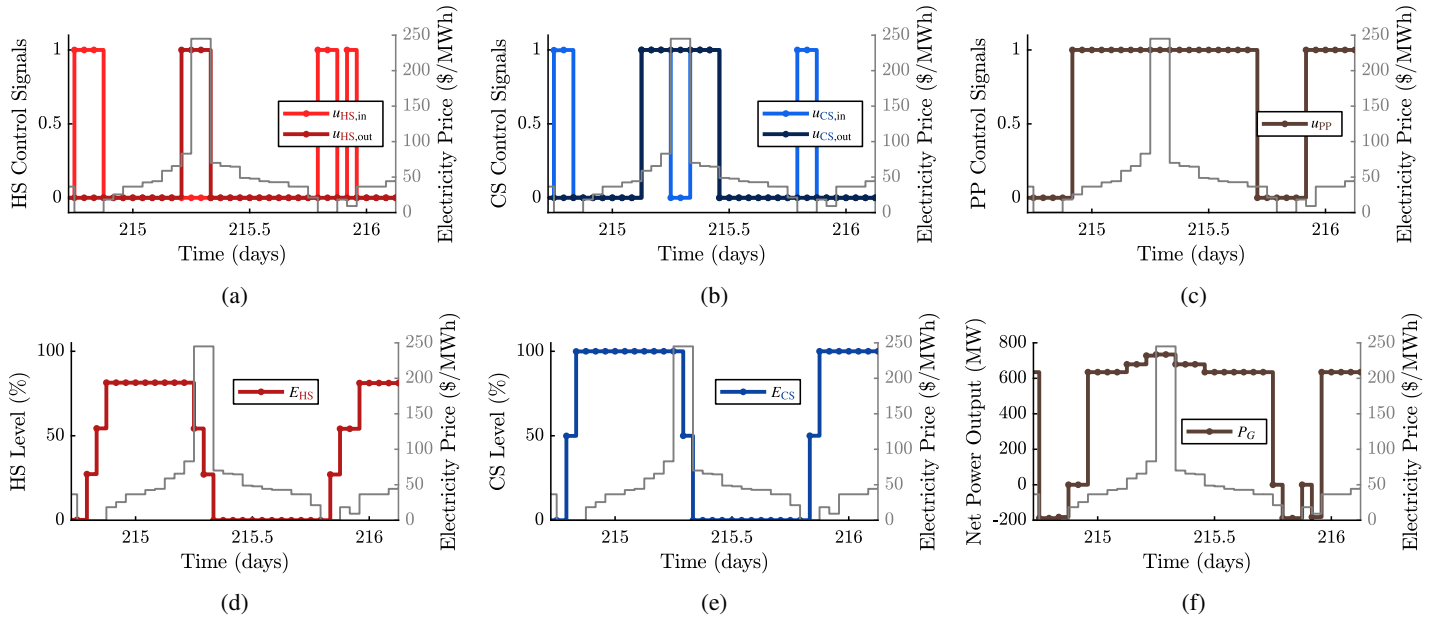

FIGURE 4: Snippet of an entire year's solution illustrating the control, states, and net power output.

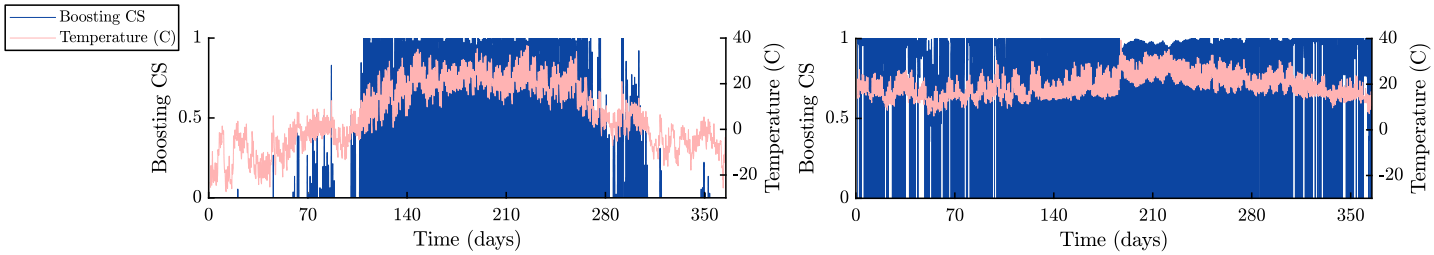

FIGURE 5: CS boosting operation for two different locations demonstrating temperature-dependent optimal operation.

program takes between 20 and 50 s[1]. Using the moving prediction horizons approach for a fixed plant, prediction horizon of 24 hours, and control window of 12 hours, the computational cost is around 13 s and varies slightly depending on the moving horizon parameters. These computational times are reasonable for online implementation at the time scales considered.

4.1 Control Strategy Results

The results presented in this section describe the workings of the control optimization to maximize NPV. In Fig. 4, a snippet of 33.5 hours of operation is shown from a year-long solution (i.e., prices and other signals are known and the controls must be determined simultaneously for an entire year) with hourly time resolution. Figures 4a–4c show all 5 of the control variables ($\boldsymbol{u}$ from Eq. (41)) governing the system, normalized with respect to their upper bounds (e.g., $u_{\text{HS,in}} = p_{\text{HS,in}}/(\mu_{\text{HS,in}} \cdot P_{\text{HS,in}})$). Figures 4d–4e respectively show the HS and CS level, two state variables in the model (see Eq. (42)). Finally, Fig. 4f shows the net power output to the grid, in which we can recognize several discrete and typical operation modes.

In the first few hours, while the electricity prices are lowest, both the HS and CS units are being charged as the normalized control variables ($u_{\text{HS,in}}, u_{\text{CS,in}}$) are equal to unity in Figs. 4a–4b, and the TES units levels ($E_{\text{HS}}, E_{\text{CS}}$) in Fig. 4d–4e increase. The TES technology configuration chosen allows for charging while the PP is offline, and that is why in this mode, the control variable to the PP ($\boldsymbol{u}_{\text{PP}}$) is equal to zero in Fig. 4c and the net power output in Fig. 4e is negative, meaning that electricity is consumed from the grid rather than delivered. Successively, after one time-interval in which the entire system is offline, the PP goes online in neutral mode for a few time-steps, which is represented by $u_{\text{PP}} = 1$ and all other control variables equal to zero.

[1]The computer architecture was a desktop workstation with an AMD 3970X CPU at 3.7 GHz and 128 GB 3200 MHz RAM.

Then, when electricity prices are higher, it becomes profitable to access the system's boosting mode, which consists in charging and discharging the CS at the same time (i.e., $u_{CS,in} = u_{CS,out} = 1$ in Fig. 4b). Because the power increase from discharging the CS is larger than the penalty for charging it, the boosting mode results in a slight increase in the system's net power output as compared with the PP neutral mode. In principle, the model does not prevent the HS from also operating in boosting mode, but because the HS generally requires more power to charge than it can generate, the boosting mode is only effective with the CS.

In the region of the plots where the electricity prices are highest, both TES units are depleted to output the maximum amount of power to the grid. This is shown by the larger power output in Fig. 4e, by the control variables ($u_{HS,out}, u_{CS,out}$) being equal to unity in Figs. 4a–4b, and by the TES levels decreasing in Figs. 4d–4e. Successively, as the electricity prices are still high but the TES units are depleted, the system is again operated in boosted mode before descending back to neutral and finally beginning another charging cycle with the PP off.

4.2 Temperature-Dependence Results

We now look at validating temperature dependence within the model and show the impact of location characteristics on the examined system. Temperature dependence was included in the model to represent the systems more accurately in real-world scenarios; it is known that power generation systems like NGCC power plants are susceptible to ambient conditions [47]. In addition, the operation of the TES units is also impacted by temperature. In particular, concerns regarding the effectiveness of CS operating at temperatures below a certain design point can be investigated using this model.

Cold Storage Operation Validation—A concern regarding the CS operation at temperatures below its design point is in the potential for ice formation in the ducting and physical damage to the unit. As a safe assumption to avoid these issues (and as a more accurate assessment of the technology in colder climates), CS utilization is limited to temperatures above 0°C, with partial restrictions from 0°C to the system's design point (15°C). Figure 5 validates the implementation of this assumption in the model; it shows the signal to use the CS boosting mode in two very different US geographical locations (Fargo and San Diego), during a year-long operation period. The market signals provided to generate these sets of results are identical, as well as the plant design; only the temperature signals identifying each of the US locations are different. With these assumptions, it is shown that a system deployed in Fargo, which is described by large seasonal temperature fluctuations and remarkably cold winters, will only be able to access the CS full capabilities during the warmer summer months. On the other hand, in a location like San Diego, the CS can be virtually used all year round because of its milder climate and higher temperatures.

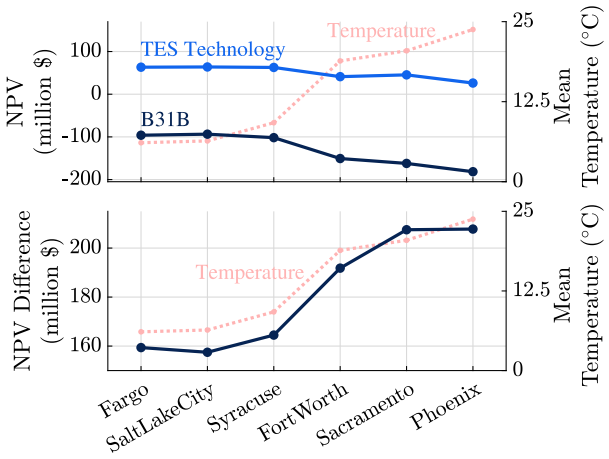

FIGURE 6: Comparing optimal net present value results for several locations and correlating them with their mean temperatures.

System Performance Validation—The entire system is expected to be affected by ambient temperature, not just the CS. In particular, the efficiency of the PP and the HS are expected to significantly decrease as temperature increases and this characteristic has been integrated within the model. Figure 6 shows the impact of temperature on the NPV of both a PP with CC and TES, as well as a base plant which is equipped with CC but no TES (denoted B31B). For this study, the techno-economic input signals are kept the same, while recorded time-varying temperature signals are selected to represent the US cities shown.

For these results, CCD optimization was conducted to make a fair assessment of these systems' optimal design decisions and performance depending on their location. As shown in Fig. 6, while NPV's for both B31B and the TES configuration noticeably decrease in warmer climates, the difference between the PP equipped with TES and the base plant tends to increase with average temperature. This trend is generally observed in Fig. 6, although since the model evaluates the effects of temperature at each time step, it is the entire temperature distribution affecting the performance of the system rather than just the mean value. For example, the system might perform better in Fargo than in Salt Lake City, despite the higher average annual temperature in the latter location.

4.3 Moving Prediction Horizons Strategy Results

Introduced in Sec. 3, a moving prediction horizons (MPH) is a pragmatic approach to the control of the system discussed in this article involving limited future foresight of the techno-economic signals upon which the optimal control strategy depends. Nonetheless, we will show that under realistic circumstances, the MPH approach ensures an economic performance extremely close to the results with perfect foresight and could be a suitable candidate for online control operation of an NGCC

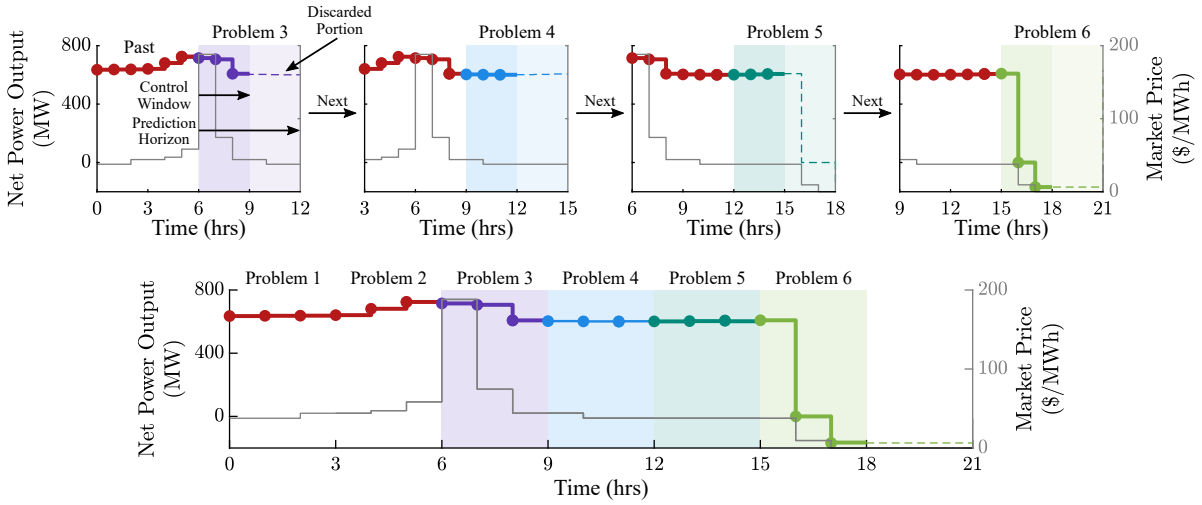

FIGURE 7: Illustration of the moving prediction horizon approach with a prediction window of 6 hours and control window of 3 hours.

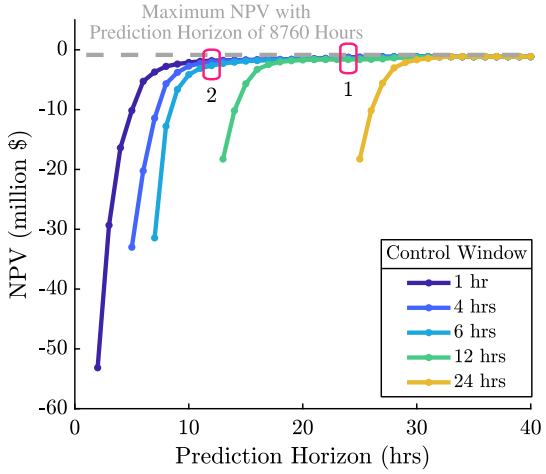

FIGURE 8: Net present value results for various prediction horizon and control window lengths in the moving prediction horizon approach compared to the maximum NPV for this scenario.

plant with CC and TES.

First, to better illustrate an MPH solution, Fig. 7 shows the net power output of the system for a few time intervals. The top row shows four successive intervals, each with its own control trajectory. The optimal strategy is computed for a total of 6 hours in advance (prediction horizon) but is updated every 3 hours (control window) because it is assumed that new information about the market is provided. On the bottom, the four intervals plotted above are shown as they compose the complete control strategy.

In Fig. 8, we can conclude that for certain values of the prediction horizon and control window, an MPH is an effective strategy for this system. Several different control window lengths were examined, and we observe NPV convergence towards the best possible value (simultaneous optimization of the entire year, i.e., prediction horizon is 8760 hours) in all cases. Marked with '1' in the figure, assuming accurate estimates of the electricity prices are available 24 hours in advance (which is usually true in most markets), we can observe solutions with control windows between 1–12 hours are close to the maximum NPV line. Even if signals are available only half a day in advance (i.e., 12-hr prediction horizon, marked with '2' in the figure), any strategy with a smaller control window still performs well. The success of the MPH approach can at least partially be explained by the general daily periodic nature of electricity prices, as well as by the TES capacities usually encountered by these systems being rarely above 10 hours. Due to these two factors, not much prior knowledge of future signals is required to operate this system effectively.

4.4 TES Technology Comparison Results

One of the more valuable features of the optimization model described in this paper is its versatility assessing a wide range of different PP, CC, HS, and CS technologies without much additional work. Here, we demonstrate this versatility with the assessment of two TES technology configurations compared with NETL's NGCC plant with CC (B31B). These configurations are examined using four future market scenarios provided by the Princeton capacity expansion model [44].

The TES configurations examined are based on different thermodynamic principles, which result in some different operational constraints. The 'IPTE' configuration is constructed by integrating B31B with an HS unit which is charged by directly pulling steam from the PP. This configuration requires the PP to be online to operate in this mode. Conversely, the 'ER' con-

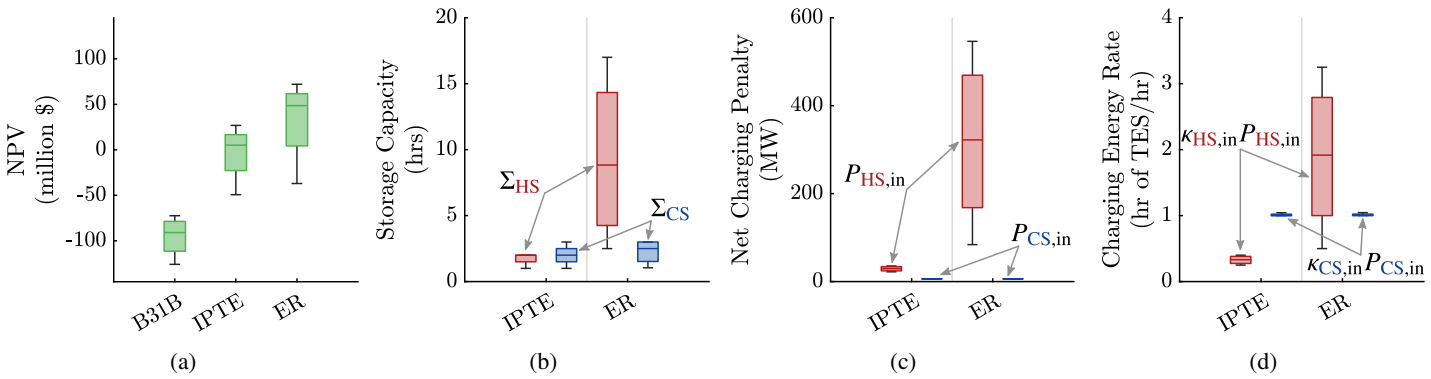

FIGURE 9: Comparing three different system configurations under several market scenarios including (a) net present value; (b) optimal storage capacities Σ_{HS} and Σ_{CS}; (c) optimal TES charging power penalties $P_{HS,in}$ and $P_{HS,in}$; and (d) equivalent optimal thermal energy transfer to the TES units.

figuration uses resistive heating and electricity either from the grid or subtracted from the NGCC gross output to charge its HS. For this reason, while the ER HS unit inflicts a more significant power penalty for charging (89% more than IPTE), it has the advantage of being able to charge while the PP is offline and to be significantly cheaper in terms of HS medium cost (by 78%). Conversely, the CS is similar for both TES configurations: it is based on an ammonia vapor compression cycle powered through electricity, and it can therefore also be charged independently of the PP. These extra operational degrees of freedom are implemented in the model by removing the inequality constraints in Eq. (16a). Again, see App. A.1 for the parameters defining each configuration. For additional details on the specific technologies and their modeling, see Refs. [18, 19].

Figure 9a compares the optimal NPV of the technologies across the market scenarios. Although we notice a relatively wide range of results, ER appears to be consistently the most profitable configuration analyzed, which can be explained by both its relatively low capital investment and the optimal plant sizing decisions shown in Figs. 9b and 9c. The storage capacity values in Fig. 9b are represented in units of time, after being normalized with respect to the power required to run the HS and CS.

We first notice how the HS design decisions are significantly different between the IPTE and ER configurations and generally point towards a much larger optimal storage capacity and net charging power penalty for the HS ($P_{HS,in}$) for the latter. This observation can be explained by: 1) the lower cost for the ER's HS medium, and 2) its ability to charge independently of the plant coupled with the nature of future electricity prices. The latter reason is particularly insightful in the context of future electricity markets with high renewable penetration: the higher penalty associated with charging the ER becomes irrelevant when the electricity prices are close to zero due to renewable's overgeneration [19]. Under these conditions, the overgenerated electricity can be stored directly from the grid within a large HS and at a high rate (demonstrated by large optimal HS normalized charging energy rate in Fig. 9d to then take advantage of when the renewables are offline, and the prices are peaking. For CS, the results for the two different configurations do not vary much as the CS unit is similar in both. A set of plant optimization variables is not shown in Fig. 9, namely the maximum energy transfer rates out of the TES units $P_{HS,out}$ and $P_{CS,out}$: under the current assumptions, their optimal value was always the maximum allowed.

Many other configurations and market scenarios were explored using this CCD optimization model in Refs. [18, 19].

5 CONCLUSION

In this work, an optimization model was constructed to help address important design and operation questions for a novel system combining natural gas power plants with carbon capture and thermal energy storage. The need for integrated design, control co-design in particular, is demonstrated for the considered system.

The thermal energy storage elements and power plant require a dynamical approach and how they are exercised is a critical decision that affects profitability and overall technology assessment. The proposed open-loop optimal control problem for this system is efficiently solved as a large-sparse linear program for an entire year at once or utilizes a more realistic, information-limited moving prediction horizons approach to investigate implementable operation. Optimal control of the system is generally not enough to realize its full economic potential due to several critical plant decisions, including storage capacities and maximum energy transfer rates. Often driven by trade-offs in their capital cost versus the additional profit attained, the optimal plant sizing decisions change depending on the configuration and

environmental signals such as (both current and future) electricity prices and location temperature.

Future work will explore how to better characterize uncertainties in the economic and environmental signals and include them as part of an implementable control strategy using moving prediction horizons. Additionally, data generated from these studies will be analyzed to better understand optimal operation, potentially leading to feedback control solutions. Overall, systematic and effective optimization-based decision support is necessary to make a fair assessment of this technology, especially considering the magnitude of the economics.

ACKNOWLEDGMENT

The information, data, or work presented herein was funded in part by the Advanced Research Projects Agency-Energy (ARPA-E), U.S. Department of Energy, under Award # DE-AR0001306.

REFERENCES

[1] International Energy Agency, 2021. Net zero by 2050: a roadmap for the global energy sector. Tech. rep., IEA, Paris, France.

[2] International Energy Agency, 2021. World energy outlook 2021. Tech. rep., IEA, Paris, France.

[3] Stark, C., Pless, J., Logan, J., Zhou, E., and Arent, D. J., 2015. Renewable electricity: insights for the coming decade. Tech. Rep. NREL/TP-6A50-63604, Joint Institute for Strategic Energy Analysis, Golden, CO, USA, Feb. doi: 10.2172/1176740

[4] Wong, D. S. H., and Jang, S., 2017. *Plantwide design and operation of CO_2 capture using chemical absorption*. Process Systems and Materials for CO_2 Capture: Modelling, Design, Control and Integration. Wiley, ch. 16, pp. 427–445. doi: 10.1002/9781119106418.ch16

[5] Lund, P. D., Lindgren, J., Mikkola, J., and Salpakari, J., 2015. "Review of energy system flexibility measures to enable high levels of variable renewable electricity". *Renew. Sust. Energ. Rev.,* ***45***, May, pp. 785–807. doi: 10.1016/j.rser.2015.01.057

[6] Dowell, N. M., and Shah, N., 2017. *Multi-period design of carbon capture systems for flexible operation*. Process Systems and Materials for CO_2 Capture: Modelling, Design, Control and Integration. Wiley, ch. 17, pp. 447–462. doi: 10.1002/9781119106418.ch17

[7] Hanak, D. P., and Manovic, V., 2020. "Linking renewables and fossil fuels with carbon capture via energy storage for a sustainable energy future". *Front. Chem. Sci. Eng.,* ***14***(3), pp. 453–459. doi: 10.1007/s11705-019-1892-2

[8] Babaee, S., and Loughlin, D. H., 2018. "Exploring the role of natural gas power plants with carbon capture and storage as a bridge to a low-carbon future". *Clean Technol. Environ. Policy,* ***20***, pp. 379–391. doi: 10.1007/s10098-017-1479-x

[9] Wilcox, J., 2012. *Carbon Capture*. Springer. doi: 10.1007/978-1-4614-2215-0

[10] Center for Climate and Energy Solutions, 2013. Leveraging natural gas to reduce greenhouse gas emissions. Tech. rep., C2ES, June.

[11] Alizadeh, M. I., Moghaddam, M. P., Amjady, N., Siano, P., and El-Eslami, M. K. S., 2016. "Flexibility in future power systems with high renewable penetration: a review". *Renew. Sust. Energ. Rev.,* ***57***, May, pp. 1186–1193. doi: 10.1016/j.rser.2015.12.200

[12] Psarras, P., He, J., Pilorgé, H., McQueen, N., Jensen-Fellows, A., Kian, K., and Wilcox, J., 2020. "Cost analysis of carbon capture and sequestration from U.S. natural gas-fired power plants". *Environ. Sci. Technol.,* ***54***(10), pp. 6272–6280. doi: 10.1021/acs.est.9b06147

[13] Singh, A., and Stéphenne, K., 2014. "Shell Cansolv CO_2 capture technology: achievement from first commercial plant". *Energy Proced.,* ***63***, pp. 1678–1685. doi: 10.1016/j.egypro.2014.11.177

[14] Bui, M., et al., 2018. "Carbon capture and storage (CCS): the way forward". *Energy Environ. Sci.,* ***11***(5), pp. 1062–1176. doi: 10.1039/c7ee02342a

[15] Abdilahi, A. M., Mustafa, M. W., Abujarad, S. Y., and Mustapha, M., 2018. "Harnessing flexibility potential of flexible carbon capture power plants for future low carbon power systems: review". *Renew. Sust. Energ. Rev.,* ***81***(2), Jan., pp. 3101–3110. doi: 10.1016/j.rser.2017.08.085

[16] Goto, K., Yogo, K., and Higashii, T., 2013. "A review of efficiency penalty in a coal-fired power plant with post-combustion CO_2 capture". *Appl. Energy,* ***111***, Nov., pp. 710–720. doi: 10.1016/j.apenergy.2013.05.020

[17] Cohen, S. M., Rochelle, G. T., and Webber, M. E., 2011. "Optimal operation of flexible post-combustion CO_2 capture in response to volatile electricity". *Energy Proced.,* ***4***, pp. 2604–2611. doi: 10.1016/j.egypro.2011.02.159

[18] Limb, B. J., Markey, E., Vercellino, R., Garland, S., Pisciotta, M., Psarras, P., Herber, D. R., Bandhauer, T., and Quinn, J. C. "Economic viability of thermal energy storage on natural gas power plants with carbon capture". *(submitted to) J. Energy Storage*.

[19] Markey, E., 2022. "Economic impact of resistively heated hot thermal storage and vapor compression cold thermal storage on natural gas power with carbon capture in future electricity markets". M.S. Thesis, Colorado State University, Fort Collins, CO, USA.

[20] Herber, D. R., and Allison, J. T., 2019. "Nested and simultaneous solution strategies for general combined plant and control design problems". *J. Mech. Design.,* ***141***(1), Jan., p. 011402. doi: 10.1115/1.4040705

[21] Thokar, R. A., Gupta, N., Niazi, K. R., Swarnkar, A., and Meena, N. K., 2021. "Multiobjective nested optimization framework for simultaneous integration of multiple photovoltaic and battery energy storage systems in distribution networks". *J. Energy Storage,* ***35***, Mar. doi: 10.1016/j.est.2021.102263

[22] Aghajani, A., Kazemzadeh, R., and Ebrahimi, A., 2018. "Optimal energy storage sizing and offering strategy for the presence of wind power plant with energy storage in the electricity market". *Int. Trans. Electr. Energy Syst.,* ***28***(11). doi: 10.1002/etep.2621

[23] Miao, Y., Chen, T., Bu, S., Liang, H., and Han, Z., 2021. "Co-optimizing battery storage for energy arbitrage and frequency regulation in real-time markets using deep reinforcement learning". *Energies,* ***14***(24). doi: 10.3390/en14248365

[24] Li, D., Wu, J., Zhang, J., and Wang, P., 2021. "Co-design optimization of a combined heat and power hybrid energy system". In International Design Engineering Technical Conferences, no. DETC2021-71304. doi: 10.1115/DETC2021-71304

[25] Liu, F., Zhu, W., and Zhao, J., 2018. "Model-based dynamic optimal control of a CO_2 heat pump coupled with hot and cold thermal storages". *Appl. Therm. Eng.,* ***128***, Jan., pp. 1116–1125. doi: 10.1016/j.applthermaleng.2017.09.098

[26] Blarke, M. B., Yazawa, K., Shakouri, A., and Carmo, C., 2012. "Thermal battery with CO_2 compression heat pump: techno-economic optimization of a high-efficiency smart grid option for buildings". *Energy Build.,* ***50***, July, pp. 128–138. doi: 10.1016/j.enbuild.2012.03.029

[27] Campos, G., Liu, Y., Schmidt, D., Yonkoski, J., Colvin, D., Trombly, D., El-Farra, N., and Palazoglu, A., 2021. "Optimal real-time dispatching of chillers and thermal storage tank in a university campus central plant". *Appl. Energy,* ***300***, p. 117389. doi: 10.1016/j.apenergy.2021.117389

[28] Falugi, P., O'Dwyer, E., Zagorowska, M. A., Atam, E., Kerrigan, E. C., Strbac, G., and Shah, N., 2022. *MPC and optimal design of residential buildings with seasonal storage: a case study*. Springer, pp. 129–160. doi: 10.1007/978-3-030-79742-3_6

[29] Yuan, M., Teichgraeber, H., Wilcox, J., and Brandt, A. R., 2019. "Design and operations optimization of membrane-based flexible carbon capture". *Int. J. Greenh. Gas Control,* ***84***, May, pp. 154–163. doi: 10.1016/j.ijggc.2019.03.018
[30] Sahraei, M. H., and Ricardez-Sandoval, L. A., 2014. "Controllability and optimal scheduling of a CO_2 capture plant using model predictive control". *Int. J. Greenh. Gas Control,* ***30***, Nov., pp. 58–71. doi: 10.1016/j.ijggc.2014.08.017
[31] Fernando, J., 2021. Net present value (NPV). Online. url: https://www.investopedia.com/terms/n/npv.asp
[32] Garrett, S. J., 2015. "Chapter 5 - sequences and series". In *Introduction to Actuarial and Financial Mathematical Methods*. Academic Press, pp. 147–191. doi: 10.1016/B978-0-12-800156-1.00005-4
[33] Herber, D. R., 2017. "Advances in combined architecture, plant, and control design". Ph.D. Dissertation, University of Illinois at Urbana-Champaign, Urbana, IL, USA, Dec.
[34] Kelly, M., 2017. "An introduction to trajectory optimization: how to do your own direct collocation". *SIAM Rev.,* ***59***(4), Jan., pp. 849–904. doi: 10.1137/16M1062569
[35] Betts, J. T., 2010. *Practical Methods for Optimal Control and Estimation Using Nonlinear Programming*. SIAM. doi: 10.1137/1.9780898718577
[36] DTQP project. url: https://github.com/danielrherber/dt-qp-project
[37] linprog. Online. url: https://www.mathworks.com/help/optim/ug/linprog.html
[38] New York ISO. Energy market & operational data. Online. https://www.nyiso.com/energy-market-operational-data
[39] Rawlings, J. B., Mayne, D. Q., and Diehl, M. M., 2020. *Model Predictive Control: Theory, Computation, and Design*, 2nd ed. Nob Hill Publishing.
[40] Sundarrajan, A. K., and Herber, D. R., 2021. "Towards a fair comparison between the nested and simultaneous control co-design methods using an active suspension case study". In American Control Conference. doi: 10.23919/ACC50511.2021.9482687
[41] Nash, A. L., Pangborn, H. C., and Jain, N., 2021. "Robust control co-design with receding-horizon MPC". In American Control Conference. doi: 10.23919/ACC50511.2021.9483216
[42] Deshmukh, A. P., Herber, D. R., and Allison, J. T., 2015. "Bridging the gap between open-loop and closed-loop control in co-design: a framework for complete optimal plant and control architecture design". In American Control Conference, pp. 4916–4922. doi: 10.1109/ACC.2015.7172104
[43] James III, R. E., Kearins, D., Turner, M., Woods, M., Kuehn, N., and Zoelle, A., 2019. Cost and performance baseline for fossil energy plants volume 1: bituminous coal and natural gas to electricity. Tech. Rep. NETL-PUB-22638, National Energy Technology Laboratory, Sept. doi: 10.2172/1569246
[44] Jenkins, J. D., Chakrabarti, S., Cheng, F., and Patankar, N., 2021. Summary report of the GenX and PowerGenome runs for generating price series (for ARPA-E FLECCS project), Dec. doi: 10.5281/zenodo.5765798
[45] Cohen, S., and Durvasulu, V., 2021. NREL price series developed for the ARPA-E FLECCS program. doi: 10.7799/1838046
[46] National Renewable Energy Laboratory, 2018. National solar radiation database. https://nsrdb.nrel.gov
[47] Chacartegui, R., Jiménez-Espadafor, F., Sánchez, D., and Sánchez, T., 2008. "Analysis of combustion turbine inlet air cooling systems applied to an operating cogeneration power plant". *Energy Convers. Manag.,* ***49***(8), pp. 2130–2141. doi: 10.1016/j.enconman.2008.02.023
[48] National Renewable Energy Laboratory, 2020. Electricity annual technology baseline (ATB) data download. Online. url: https://atb.nrel.gov
[49] U.S. Energy Information Administration, 2021. Annual energy outlook 2021. Tech. rep., U.S. Department of Energy, Washington, DC, USA, Feb.
[50] U.S. Bureau of Labor Statistics, 2021. Consumer price index data. Online. url: https://data.bls.gov/timeseries/CUUR0000SA0

A CASE STUDY PARAMETERS

A.1 Technology Parameters

The parameters describing the technologies examined in the case studies presented in Sec. 4 are shown in Table 1. The parameters reported reference the nomenclature of the optimization model in Sec. 2 and are evaluated at 15°C.

TABLE 1: Techno-economic parameters for the technology configurations examined in the case studies.

Parameter	Units	B31B	ER	IPTE
ρf	kg NG/s/MW	0.04082	0.04082	0.04082
c_{n}		0.9	0.9	0.9
$\kappa_{\mathrm{HS,in}}$	hr TES/MW	0	0.005949	0.01126
$\kappa_{\mathrm{CS,in}}$	hr TES/MW	0	0.1609	0.1609
$\kappa_{\mathrm{HS,out}}$	hr TES/MW	0	0.02211	0.02028
$\kappa_{\mathrm{CS,out}}$	hr TES/MW	0	0.01986	0.02075
$\Delta\rho_f$	kg/s/MW	0	0.03783	0.03951
Δc_{d}		0	0.06163	0.06163
$\Delta\rho_{\mathrm{CO_2,in}}$	kg CO_2/MW	0	-0.00025	-0.00026
$\Delta\rho_{\mathrm{CO_2,out}}$	ton CO_2/MW	0	0.0067	0.0070
P_{CCT}, P_{CCE}	MW	0	0	0
α_C	ton CO_2/kg NG	0.0029	0.0029	0.0029
$\eta^\star$		1	1	1
$c_{\mathrm{PP,VOM}}$	\$/MWh	1.705	1.705	1.705
$c_{\mathrm{CC,VOM}}$	\$/ton CO_2	7.2	7.2	7.2
$c^\dagger_{\mathrm{TES,VOM}}$	\$/MWh	0	0.75	0.75
$c_{\mathrm{PP,FOM}}$	M\$/year	12.9773	12.9773	12.9773
$c_{\mathrm{CC,FOM}}$	M\$/year	14.5360	14.5360	14.5360
$c_{\mathrm{HS,in,FOM}}$	k\$/MW/year	0	2.5881	2.5881
$c_{\mathrm{CS,in,FOM}}$	k\$/MW/year	0	15.0721	0 15.0721
$c_{\mathrm{HS,out,FOM}}$	k\$/MW/year	0	4.12186	4.12186
$c_{\mathrm{CS,out,FOM}}$	k\$/MW/year	0	0.79725	0.79725
$c_{\mathrm{HS,TES,FOM}}$	k\$/hr of TES/year	0	41.9579	190.2704
$c_{\mathrm{CS,TES,FOM}}$	k\$/hr of TES/year	0	45.5942	56.9928
C_{PP}	M\$	537.7230	537.7230	537.7230
C_{CC}	M\$	743.6010	743.6010	743.6010
$c_{\mathrm{HS,in}}$	k\$/MW	0	64.7012	39.3198
$c_{\mathrm{CS,in}}$	k\$/MW	0	376.8015	376.8018
$c_{\mathrm{HS,out}}$	k\$/MW	0	103.0466	30.3505
$c_{\mathrm{CS,out}}$	k\$/MW	0	19.9311	20.8169
$c_{\mathrm{HS,TES}}$	M\$/hr of TES	0	1.048947	4.756760
$c_{\mathrm{CS,TES}}$	M\$/hr of TES	0	1.139856	1.424820
$\bar{P}_{\mathrm{PP}}$	MW	634.741	634.741	634.741
$\bar{P}_{\mathrm{HS,in}}$	MW	0	840.515	443.9915
$\bar{P}_{\mathrm{CS,in}}$	MW	0	31.06755	31.06755
$\bar{P}_{\mathrm{HS,out}}$	MW	0	45.2353	49.303
$\bar{P}_{\mathrm{CS,out}}$	MW	0	50.3432	48.2011

$^\star\eta$ is for (η_{GE}, η_{HS}, η_{CS})
$^\dagger c_{\mathrm{TES,VOM}}$ is for ($c_{\mathrm{HS,VOM}}$, $c_{\mathrm{CS,VOM}}$)

A.2 NPV Economic Assumptions

Standard economic and financial assumptions used to generate the NPV results are presented in Table 2 [48, 49]. All dollar values were adjusted to December 2018 dollars based on historical inflation rates as calculated by the Bureau of Labor Statistics using the Consumer Price Index [50].

TABLE 2: Economic assumptions for the calculation of net present value in the case studies.

Parameter	Units	Value
L_t [48]	years	30
IRR [48]		10%
i_e [49]	%/year	3.5%
i_f [49]	%/year	2.2%